REGULAR ARTICLE

blood advances

Impact of mesenchymal stromal cell–derived vesicular cargo on B-cell acute lymphoblastic leukemia progression

Christina Karantanou,[1] Valentina R. Minciacchi,[1] Rahul Kumar,[1] Costanza Zanetti,[1] Jimena Bravo,[1] Raquel S. Pereira,[1] Georg Tascher,[2] Tobias Tertel,[3] Adriana Covarrubias-Pinto,[2] Katrin Bankov,[4] Lisa-Marie Pfeffermann,[5] Halvard Bonig,[5-7] Paola Divieti-Pajevic,[8] David G. McEwan,[9] Bernd Giebel,[3] Christian Münch,[2] Ivan Dikic,[2,10] and Daniela S. Krause[1,2,6,11-13]

[1]Institute for Tumor Biology and Experimental Therapy, Georg-Speyer-Haus, Frankfurt am Main, Germany; [2]Institute of Biochemistry II, Medical Faculty, Goethe University, Frankfurt am Main, Germany; [3]Institute for Transfusion Medicine, University Hospital Essen, Essen, Germany; [4]Department of Pathology, Goethe University, Frankfurt am Main, Germany; [5]German Red Cross Blood Service Baden-Württemberg-Hessen, Institute Frankfurt, Frankfurt, Germany; [6]Institute for Transfusion Medicine and Immunohematology, Goethe University, Frankfurt, Germany; [7]Department of Medicine/Hematology, University of Washington, Seattle, WA; [8]Goldman School of Dental Medicine, Boston University, Boston, MA; [9]Cancer Research UK Beatson Institute, Glasgow, United Kingdom; [10]Buchmann Institute for Molecular Life Sciences, Frankfurt am Main, Germany; [11]Institute for General Pharmacology and Toxicology, Goethe University, Frankfurt am Main, Germany; [12]Frankfurt Cancer Institute, Frankfurt am Main, Germany; and [13]German Cancer Research Center (DKFZ), Heidelberg, Germany

Key Points

- The PLEKHM1-associated endolysosomal system in MSCs affects BCR-ABL1$^+$ B-ALL progression via release of extracellular vesicles.
- B-ALL–derived inflammatory cytokines perpetuate this circuit in MSCs, modify vesicular cargo, and promote B-ALL cell signaling and survival.

Leukemia cells reciprocally interact with their surrounding bone marrow microenvironment (BMM), rendering it hospitable to leukemia cell survival, for instance through the release of small extracellular vesicles (sEVs). In contrast, we show here that BMM deficiency of pleckstrin homology domain family M member 1 (PLEKHM1), which serves as a hub between fusion and secretion of intracellular vesicles and is important for vesicular secretion in osteoclasts, accelerates murine BCR-ABL1+ B-cell acute lymphoblastic leukemia (B-ALL) via regulation of the cargo of sEVs released by BMM-derived mesenchymal stromal cells (MSCs). PLEKHM1-deficient MSCs and their sEVs carry increased amounts of syntenin and syndecan-1, resulting in a more immature B-cell phenotype and an increased number/function of leukemia-initiating cells (LICs) via focal adhesion kinase and AKT signaling in B-ALL cells. Ex vivo pretreatment of LICs with sEVs derived from PLEKHM1-deficient MSCs led to a strong trend toward acceleration of murine and human BCR-ABL1$^+$ B-ALL. In turn, inflammatory mediators such as recombinant or B-ALL cell–derived tumor necrosis factor α or interleukin-1β condition murine and human MSCs in vitro, decreasing PLEKHM1, while increasing syntenin and syndecan-1 in MSCs, thereby perpetuating the sEV-associated circuit. Consistently, human trephine biopsies of patients with B-ALL showed a reduced percentage of PLEKHM1$^+$ MSCs. In summary, our data reveal an important role of BMM-derived sEVs for driving specifically BCR-ABL1$^+$ B-ALL, possibly contributing to its worse prognosis compared with BCR-ABL1$^-$ B-ALL, and suggest that secretion of inflammatory cytokines by cancer cells in general may similarly modulate the tumor microenvironment.

Introduction

B-cell acute lymphoblastic leukemia (B-ALL) is a hematological malignancy affecting children and adults.[1] BCR-ABL1+ B-ALL is a subtype of B-ALL accounting for 3% to 5% of pediatric and 25% of

Submitted 8 March 2022; accepted 15 August 2022; prepublished online on *Blood Advances* First Edition 31 August 2022. https://doi.org/10.1182/bloodadvances.2022007528.

All reagents and data sets are available upon request from the corresponding author, Daniela S. Krause (krause@gsh.uni-frankfurt.de).

The full-text version of this article contains a data supplement.

B-ALL cases in adults,[2] conferring a poor prognosis.[3] BCR-ABL1$^+$ B-ALL is characterized by the chromosomal translocation t(9;22), giving rise to the constitutively active tyrosine kinase BCR-ABL1.[2] Despite overall improved clinical outcomes, especially in pediatric B-ALL,[1] the incidence of relapse in BCR-ABL1$^+$, also BCR-ABL1$^-$ B-ALL, remains a concern, highlighting the need for the discovery of novel and potentially targetable mechanisms that accelerate the progression of B-ALL.[4]

The bone marrow (BM) microenvironment (BMM) supports the progression of B-ALL and other leukemias and promotes their resistance to established therapies.[5,6] Reciprocal interactions between leukemia cells and the BMM are mediated by BMM constituents, such as mesenchymal stromal cells (MSCs), osteoblasts, and other factors.[5] Although osteoclasts are considered components of the BMM, knowledge of their role in hematopoiesis has been limited to their influence on hematopoietic stem cell mobilization.[7] Only few reports have described the effects of B-ALL on bone physiology,[8,9] and overall, insight into the role of osteoclasts in B-ALL is limited.

Pleckstrin homology domain family M member 1 (PLEKHM1) is a protein that facilitates the trafficking of secretory lysosomes in osteoclasts. Mutations in *PLEKHM1* may lead to dysfunctional osteoclasts and osteopetrotic phenotypes in rats and humans.[10] In a related function, PLEKHM1 is an autophagy adapter protein mediating the fusion of autophagosomes with lysosomes[11,12] and the trafficking of endosomes,[13-15] which include multivesicular bodies (MVBs). These MVBs contain intraluminal vesicles, which, upon fusion of the MVB with the plasma membrane, are released as small extracellular vesicles (sEVs) or exosomes.[16] Therefore, we hypothesized that PLEKHM1 may influence B-ALL progression via osteoclast-mediated defects as found in osteopetrosis[10] or altered trafficking of vesicles released from osteoclasts or other cells.

Here, we identify a circular model in which TNF-α secreted from BCR-ABL1$^+$ B-ALL cells establishes a favorable niche for B-ALL progression via a reduction of PLEKHM1 in MSC and hence increased loading of MVB-derived sEVs with syntenin and syndecan-1, which are released into their extracellular environment. Uptake of these sEVs by B-ALL cells increases phosphorylation of protein kinase B (AKT) and focal adhesion kinase (FAK), promoting B-ALL cell proliferation, migration, and BCR-ABL1$^+$ B-ALL advancement. The discovered mechanism connects the endolysosomal system as a quality control pathway in cells of the tumor microenvironment with leukemia progression and may also be relevant in other nonleukemic cancer types.

Materials and methods

Induction of B-ALL

To induce BCR-ABL1$^+$ B-ALL, BM cells were harvested from wild-type (WT) mice, transduced once with MSCV IRES green fluorescent protein (GFP) BCR-ABL1–expressing retrovirus and transplanted into sublethally irradiated (2 × 450 cGy) recipient mice.[17]

Preparation of extracellular vesicles (EVs)

sEVs were obtained by differential centrifugation.[18]

Statistical analysis

Data are represented as mean ± SD and were considered statistically significant if $P \leq .05$. GraphPad Prism Software (Prism 9.0) was used for the generation of all graphs and for statistical analyses. Statistical significance was calculated using the Student *t* test, one-way or two-way analysis of variance (ANOVA). For post hoc analysis, Tukey, Sidak, or Dunnett tests were used to determine statistical significance between multiple comparisons. For survival analyses by Kaplan-Meier curves, the log-rank (Mantel-Cox) test was used.

Results

Deficiency of PLEKHM1 in the BMM accelerates B-ALL disease

To study the role of PLEKHM1 in the BMM in B-ALL, we transplanted WT murine BM, transduced with *BCR-ABL1*–expressing retrovirus, into *Plekhm1* KO (Knockout) or WT recipient mice. Comparison of the hematological profile in normal *Plekhm1* KO vs WT mice did not show differences (supplemental Figure 1A-E). Upon induction of B-ALL, a significantly increased number of leukocytes ($P = .04$; Figure 1A) and GFP$^+$ (BCR-ABL1$^+$) BP-1$^+$ pre-B cells were observed in *Plekhm1* KO compared to WT recipient mice ($P = .02$; Figure 1B). This was accompanied by significant disease acceleration in *Plekhm1* KO recipients ($P = .04$; Figure 1C). This phenotype was not due to increased homing of the BCR-ABL1$^+$ (GFP$^+$) BP-1$^+$ leukemia-initiating cells (LICs) to the BM or spleen of *Plekhm1* KO compared with WT recipient mice (Figure 1D). Nonirradiation of recipients before transplantation of B-ALL LIC[19] confirmed the increased percentage of GFP$^+$ (BCR-ABL1$^+$) cells in *Plekhm1* KO recipients (supplemental Figure 2A-B). Transplantation of 5-fluorouracil–pretreated BM, transduced with BCR-ABL1 or MLL-AF9–expressing retrovirus, to induce chronic myeloid leukemia (CML)–like myeloproliferative neoplasia or acute myeloid leukemia (AML), in contrast, revealed that *Plekhm1* KO recipient mice with CML-like myeloproliferative neoplasia showed a decreased GFP$^+$ (BCR-ABL1$^+$) CD11b$^+$ myeloid tumor burden in PB (supplemental Figure 3A) and a modest prolongation of survival compared with WT recipients (supplemental Figure 3B). No differences were observed between the 2 cohorts with regard to tumor load (supplemental Figure 3C) or overall survival in the AML model (supplemental Figure 3D).

Focusing on BCR-ABL1$^+$ B-ALL, we showed reduced early apoptosis in GFP$^+$ (BCR-ABL1$^+$) BP-1$^+$ cells from *Plekhm1* KO compared to those from WT recipient mice ($P = .02$; Figure 1E; supplemental Figure 3E). In addition, expression of the B-cell–specific markers CD19 ($P = .02$; Figure 1F) and B220 ($P = .017$; Figure 1G) was significantly reduced in GFP$^+$ (BCR-ABL1$^+$) BP-1$^+$ cells derived from *Plekhm1* KO compared to those from WT mice. Consistently, expression levels of the paired box 5 (*Pax5*) gene (*Bsap*), which encodes for a transcription factor with a key role in B-lymphocyte development[20] and CD19 expression,[21] were reduced in BM cells from *Plekhm1* KO mice ($P = .03$; Figure 1H). Proteomic analysis of GFP$^+$ (BCR-ABL1$^+$) BP-1$^+$ cells from *Plekhm1* KO mice with B-ALL revealed significantly decreased expression of the immunoglobulin heavy constant alpha 1 and immunoglobulin kappa constant proteins, both of which are

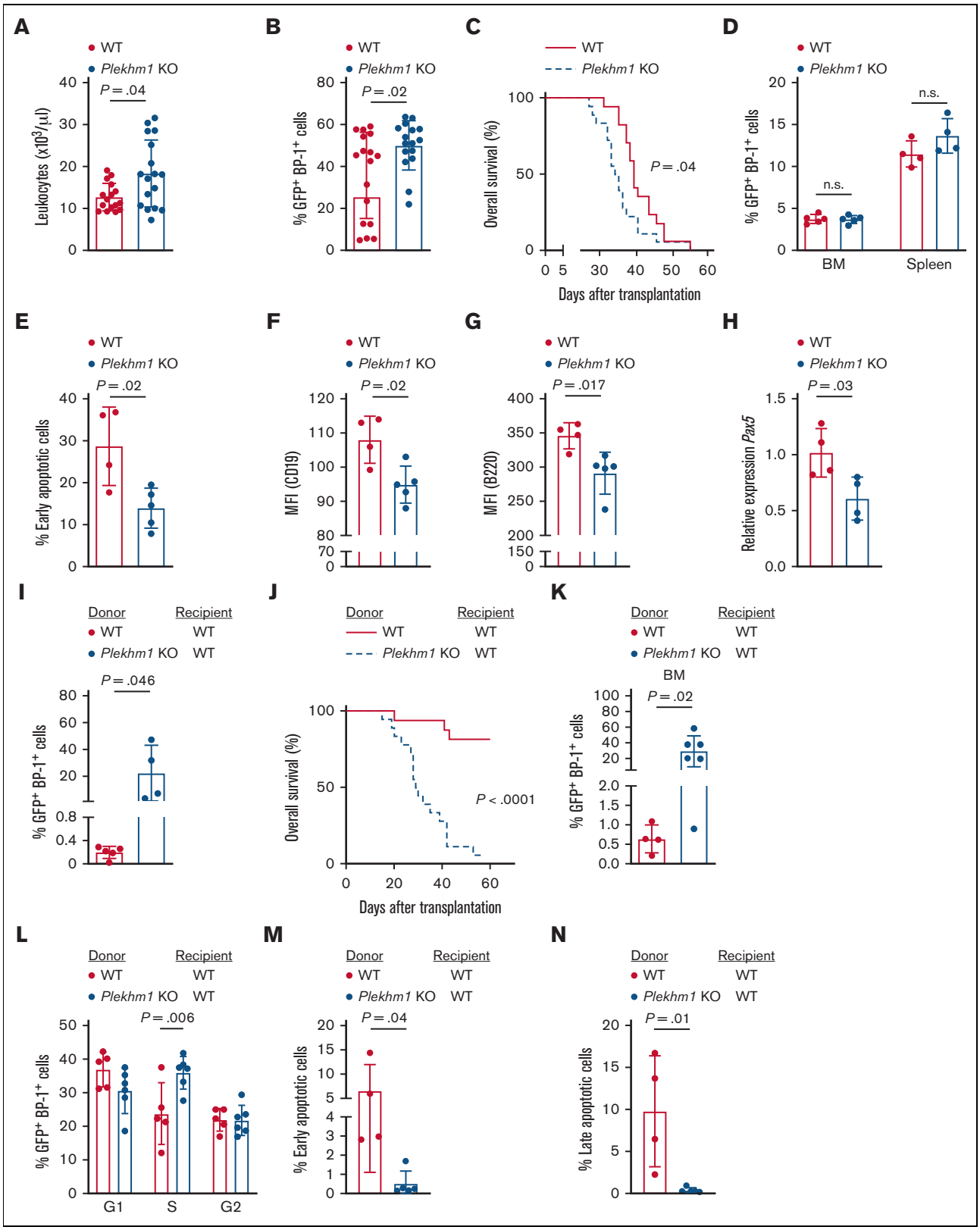

Figure 1. Deficiency of PLEKHM1 in the BMM accelerates B-ALL disease. (A) Leukocyte counts in PB of WT (red) or *Plekhm1* KO (blue) recipient mice on day 20 after transplantation with BCR-ABL1$^+$-transduced BM in the B-ALL model (WT n =16; *Plekhm1* KO n = 17; *t* test). (B) Percentage of GFP$^+$ (BCR-ABL1$^+$) BP-1$^+$ cells of single cells in PB of WT (red) or *Plekhm1* KO (blue) recipient mice of BCR-ABL1–transduced BM on day 20 after transplantation. (WT n = 17; *Plekhm* KO n = 16; test). (C) Kaplan-Meier style survival curve for WT (red solid line) or *Plekhm1* KO (blue dashed line) recipient mice with BCR-ABL1$^+$ B-ALL (WT n = 17; *Plekhm1* KO n = 18; log-rank test).

components of the B-cell receptor of mature B lymphocytes,[22] compared with WT mice (supplemental Figure 3F). This may suggest a more immature phenotype of B-ALL cells in a *Plekhm1* KO than in a WT BMM. To assess the number or function of LICs, BM cells from WT or *Plekhm1* KO mice with established B-ALL (supplemental Figure 3G) were transplanted into WT secondary recipient mice. This led to an increased tumor load in the PB ($P = .046$; Figure 1I) and a strikingly reduced overall survival ($P < .0001$; Figure 1J) of mice that had received B-ALL cells from *Plekhm1* KO compared with WT donor mice.

Mice transplanted with B-ALL cells from a *Plekhm1* KO BMM had an increased percentage of GFP$^+$ (BCR-ABL1$^+$) BP-1$^+$ cells in the BM ($P = .02$; Figure 1K). The percentage of these cells in the S phase of the cell cycle ($P = .006$; Figure 1L) was increased, and the fraction of these cells undergoing early ($P = .04$; Figure 1M) and late ($P = .01$; Figure 1N) apoptosis was decreased. In contrast, transplantation of PLEKHM1-deficient B-ALL–initiating cells led to a trend toward survival prolongation compared with recipients of WT LICs (supplemental Figure 3H).

Taken together, these data indicate that PLEKHM1 deficiency in the BMM increases B-ALL tumor load and shortens survival. This effect is more pronounced in the setting of secondary transplantation, suggesting that a *Plekhm1* KO BMM increases the number and/or function of LICs in B-ALL.

The differentiation capacity and vesicular content of *Plekhm1* KO MSC are altered

As deficiency of PLEKHM1 leads to reduced resorptive activity in osteoclasts,[10] we initially hypothesized that the shortened survival observed in *Plekhm1* KO mice with B-ALL may be due to defective osteoclasts. Therefore, we isolated monocytes from the BM of WT or *Plekhm1* KO mice and differentiated them into osteoclasts.[23] Indeed, *Plekhm1* KO osteoclasts showed reduced resorptive activity (supplemental Figure 4A). However, no differences in the proliferation of BCR-ABL1$^+$ BA/F3 cells, a frequently used in vitro model for B-ALL,[24] cultured on WT or *Plekhm1* KO osteoclasts were observed (supplemental Figure 4B), suggesting that accelerated B-ALL progression in *Plekhm1* KO mice was likely not attributable to osteoclasts. Because PLEKHM1 is also expressed in MSCs,[25] which have a known role in B-ALL,[24,26] we subsequently hypothesized that MSCs may be involved in the establishment of the observed phenotype. To address this, we isolated CD45$^-$ Ter-119$^-$ PDGFRα$^+$ Sca-1$^+$ MSC[27] from the BM of healthy WT or *Plekhm1* KO mice, which did not differ significantly with regard to the immunophenotype (supplemental Figure 4C). Testing the function and differentiation of MSCs, we found that the colony-forming ability ($P = .0002$; Figure 2A) and osteogenic differentiation potential of *Plekhm1* KO MSC were significantly higher than in WT MSCs ($P = .01$; Figure 2B). Conversely, the adipogenic differentiation potential was significantly lower ($P = .01$; Figure 2C). Given that PLEKHM1 plays a role in vesicular trafficking and fusion of late endosomes with lysosomes,[14] we further hypothesized that the reduced differentiation ability of *Plekhm1* KO MSCs into adipocytes may be associated with impairment of lipid droplet fusion. Therefore, we investigated whether the number of MVBs, a subset of specialized endosomes,[28] that is, late endosomes, differed between WT and *Plekhm1* KO MSC. Immunofluorescence staining for CD63, a marker of MVBs,[29] showed significantly increased MVBs in *Plekhm1* KO than in WT MSCs ($P = .002$; Figure 2D). Immunofluorescence for LC3-positive (autophagosomes) or LAMP1-positive vesicles (lysosomes) showed no significant differences in their number or colocalization between WT and *Plekhm1* KO MSCs (supplemental Figure 5A-D), indicative of overall similar basal levels of autophagy between WT and *Plekhm1* KO MSCs. Taken together, these results suggest that *Plekhm1* KO MSCs have an increased capacity to form colonies and a decreased capacity to differentiate into adipocytes while harboring an increased number of CD63$^+$ MVBs.

Plekhm1 KO MSC release syntenin- and syndecan-1–enriched sEVs

MVB-derived exosomes[30] are critical mediators in the communication between leukemia cells and their environment.[31,32] Given the increased number of CD63$^+$ MVBs in *Plekhm1* KO MSCs, we hypothesized that deficiency of PLEKHM1 may affect the release or content of exosomes. Using differential centrifugation, sEVs, known to be enriched in exosomes and found in the 100k

Figure 1 (continued) (D) Percentage of GFP$^+$ (BCR-ABL1$^+$) BP-1$^+$ cells of total leukocytes which homed to the BM or spleen of WT (red) or *Plekhm1* KO (blue) recipient mice 18 hours after transplantation (BM: WT n = 5; *Plekhm1* KO n = 5; spleen: WT n = 4; *Plekhm1* KO n = 4; multiple *t* tests). (E) Percentage of GFP$^+$ (BCR-ABL1$^+$) BP-1$^+$ early apoptotic (DAPI AnnV) cells of single cells in the BM of WT (red) or *Plekhm1* KO (blue) mice with B-ALL on day 20 after transplantation (WT n = 4; *Plekhm1* KO n = 5; *t* test). (F) MFI of CD19 in GFP$^+$ (BCR-ABL1$^+$) cells in the BM of WT (black) or *Plekhm1* KO (gray) mice with BCR-ABL1$^+$ B-ALL on day 20 after transplantation (WT n = 4; *Plekhm1* KO n = 5; *t* test). (G) MFI of B220 in GFP$^+$ (BCR-ABL1$^+$) cells in the BM of WT (red) or *Plekhm1* KO (blue) mice with BCR-ABL1$^+$ B-ALL on day 20 after transplantation (WT n = 4; *Plekhm1* KO n = 5; *t* test). (H) Relative expression of *Pax5* in total BM of WT (red) or *Plekhm1* KO (blue) mice with BCR-ABL1$^+$ B-ALL on day 20 after transplantation (WT n = 4; *Plekhm1* KO n = 4; *t* test). (I) Percentage of GFP$^+$ (BCR-ABL1$^+$) BP-1$^+$ cells of single cells in the PB of WT secondary recipient mice of total BM cells from WT (red) or *Plekhm1* KO (blue) donor mice with established B-ALL. Cells were analyzed on day 20 after transplantation (WT n = 5; *Plekhm1* KO n = 4; *t* test). (J) Kaplan-Meier style survival curve of WT secondary recipients of total BM cells from WT (red solid line) or *Plekhm1* KO (blue dashed line) donor mice with established B-ALL (WT n = 16; *Plekhm1* KO n = 17; log-rank test). (K) Percentage of GFP$^+$ (BCR-ABL1$^+$) BP1$^+$ cells of single cells in the BM of WT secondary recipients of total BM cells from WT (red) or *Plekhm1* KO (blue) donor mice with established B-ALL. Cells were analyzed on day 20 after transplantation (WT n = 4; *Plekhm1* KO n = 6; *t* test). (L) Percentage of GFP$^+$ (BCR-ABL1$^+$) BP-1$^+$ cells of single cells in the G1, S, or G2 phases of the cell cycle in the BM of WT secondary recipients of total BM cells from WT (red) or *Plekhm1* KO (blue) donor mice with established B-ALL. Cells were analyzed on day 20 after transplantation (WT n = 5; *Plekhm1* KO n = 6; two-way ANOVA, Sidak multiple comparisons test). (M) Percentage of GFP$^+$ (BCR-ABL1$^+$) BP-1$^+$ early apoptotic (DAPI$^-$ AnnV$^+$) cells of single cells in the BM of WT secondary recipients of total BM cells from WT (red) or *Plekhm1* KO (blue) donor mice with established B-ALL. Cells were analyzed on day 20 after transplantation (WT n = 4; *Plekhm1* KO n = 5; *t* test). (N) Percentage of GFP$^+$ (BCR-ABL1$^+$) BP1$^+$ late apoptotic (DAPI$^+$ AnnV$^+$) cells of single cells in the BM of WT secondary recipients of total BM cells from WT (red) or *Plekhm1* KO (blue) donor mice with established B-ALL. Cells were analyzed on day 20 after transplantation (WT n = 4; *Plekhm1* KO n = 5; *t* test). DAPI, 4′, 6-diamidino-2-phenylindole; MFI, mean fluorescence intensity; PB, peripheral blood.

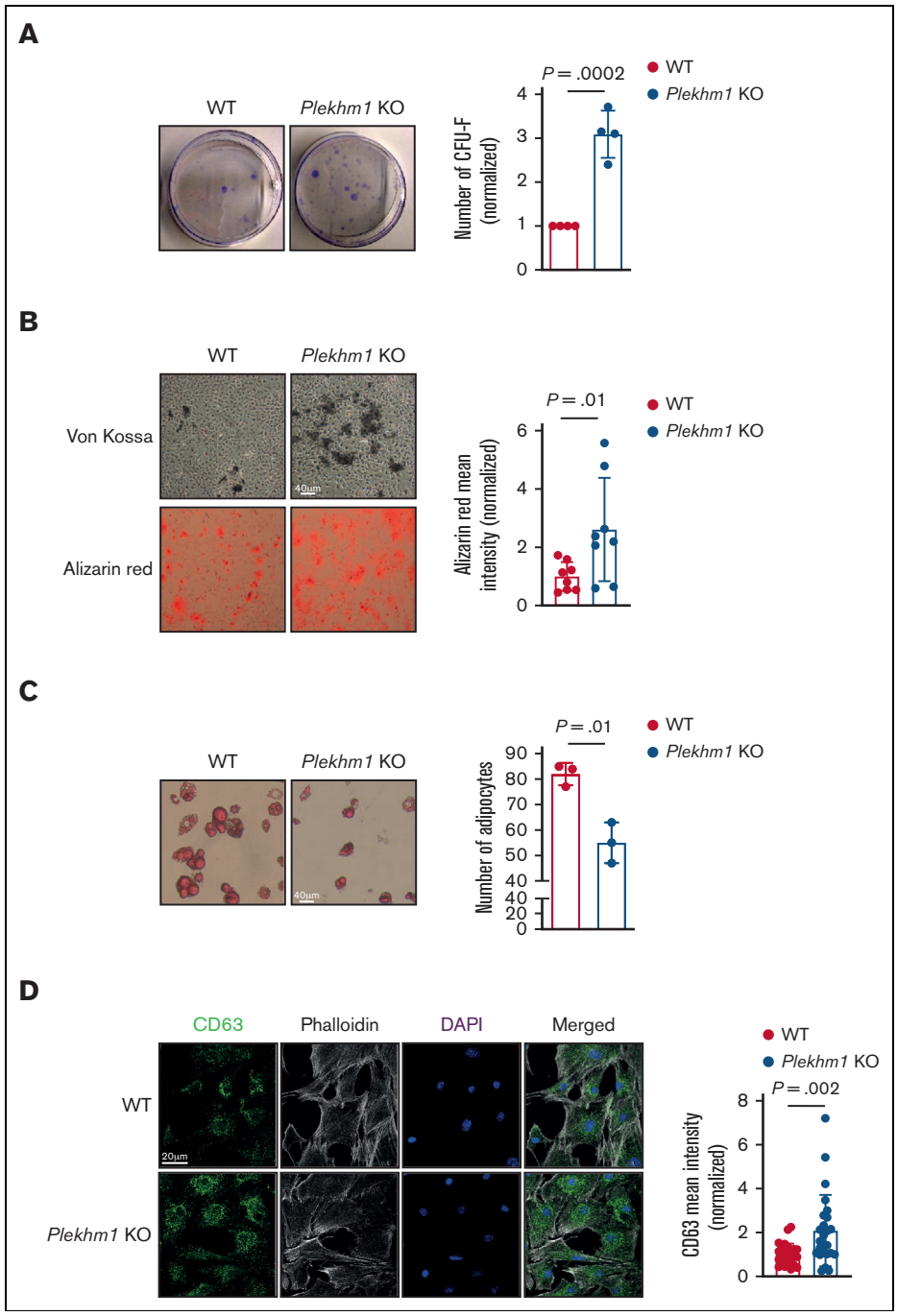

Figure 2. The differentiation capacity and vesicular content of *Plekhm1* KO MSC are altered. (A) Representative images of colonies derived from WT or *Plekhm1* KO MSCs, stained with crystal violet (left). Number of colonies formed by WT (red) vs *Plekhm1* KO (blue) MSCs (right). The data represent results from 4 independent experiments, and the values are normalized to the WT for each independent experiment (*t* test). (B) Osteogenic differentiation of WT or *Plekhm1* KO MSC, visualized by Von Kossa and alizarin red staining for the detection of calcium deposits (left). The scale bar depicts 40 μm. Quantification of the alizarin red staining intensity normalized by the average value of WT (right). Each dot represents a technical replicate from a total of 3 independent experiments (*t* test). (C) Adipogenic differentiation of WT or *Plekhm1* KO MSCs, visualized by oil red O staining for the detection of intracytoplasmic lipid-rich droplets in adipocytes (left). The scale bar depicts 40 μm. Quantification of the number of adipocytes formed after differentiation of WT (red) or *Plekhm1* KO (blue) MSCs (right). The data represent the results from 3 independent experiments (*t* test). (D) Representative immunofluorescence images of WT or *Plekhm1* KO MSCs stained with an antibody to CD63 (green). The nuclei are counterstained with DAPI (blue) and the cytoplasm with phalloidin (gray) (left). The scale bar depicts 20 μm. Quantification of the CD63 fluorescence intensity of WT (red) or *Plekhm1* KO (blue) MSCs (right). The values are normalized to the average value of WT. The data represent the results from 4 independent experiments (*t* test). DAPI, 4′,6-diamidino-2-phenylindole.

fraction,[18,33] were isolated from the conditioned medium of WT or *Plekhm1* KO MSCs. We confirmed the successful isolation of sEVs by the expression of the exosomal markers CD81 and flotillin-1 in the sEV preparation, as well as by the absence of expression of the Golgi matrix protein 130 kD (GM130; Golgin A2)[34] (Figure 3A). Gradient centrifugation, in contrast, led to significant loss of material and, therefore, could not be used for this study, but revealed differential enrichment of CD81 and flotillin-1 in the 10% and 15% gradient for exosomes from WT vs the 25% gradient for exosomes from *Plekhm1* KO MSCs (supplemental Figure 6A). The amount of CD81 protein (Figure 3A; supplemental Figure 6B) and the number of CD81$^+$ EVs being detected by imaging flow cytometric analysis at the single EV level[35] (Figure 3B; supplemental Figure 6C) were similar, regardless of whether the EVs were derived from MSCs from WT or *Plekhm1* KO mice (hereafter called WT and *Plekhm1* KO sEVs, respectively). Consistently, molecules of equivalent soluble fluorochrome, describing the amount of antibody bound to CD81 per sEV, were also similar between sEVs derived from WT and *Plekhm1* KO MSCs (supplemental Figure 6D). In addition, the distribution in respective cell cycle stages was similar between WT and *Plekhm1* KO MSCs (supplemental Figure 6E). Proteomic analysis of prepared sEV samples showed increased levels of vacuolar protein sorting 23 (TSG101) and vacuolar protein sorting 28 in sEV preparations from *Plekhm1* KO compared with WT MSCs (Figure 3C). Both identified proteins belong to the endosomal sorting complex required for transport (ESCRT) complex I (ESCRT-I)[36] and are responsible for the formation and sorting of cargo in intraluminal vesicles. Similarly, syntenin, which is involved in ESCRT-dependent exosomal biogenesis,[37] was also found to be significantly increased in *Plekhm1* KO sEV preparations (Figure 3C). Immunoblot analysis confirmed the enrichment of syntenin in *Plekhm1* KO sEV preparations (Figure 3D). Syntenin directly interacts with syndecan-1, a heparan sulfate proteoglycan and integral membrane protein[37] present in both healthy and tumor cells, including leukemia cells.[38] Consistent with the enrichment of syntenin, we also observed increased syndecan-1 protein levels in *Plekhm1* KO sEV preparations (Figure 3D; supplemental Figure 6F). Immunoblot analysis of MSCs, that is, the donor cells of sEVs, similarly revealed an enrichment of syntenin and syndecan-1 in *Plekhm1* KO compared with WT MSCs ($P = .049$ [syntenin], $P = .043$ [syndecan-1]; Figure 3E). Increased levels of syndecan-1 were also confirmed in *Plekhm1* KO MSCs ($P = .01$; Figure 3F). These findings are consistent with reports that the overexpression of the cytoplasmic adapter molecule syntenin and syndecan-1 in donor cells may enhance their exosomal expression.[37] Our data suggest that deficiency of PLEKHM1 leads to increased levels of syntenin and syndecan-1 in MSCs and MSC-derived sEVs, while leaving numbers of released sEVs unaffected.

sEVs derived from *Plekhm1* KO MSCs alter signaling in B-ALL cells and may promote B-ALL progression

Given the differences in the cargo of sEVs from *Plekhm1* KO and WT MSCs, we tested the effect of the obtained sEV preparations on B-ALL target cells. Indeed, exposure of BCR-ABL1$^+$ BA/F3 cells to *Plekhm1* KO sEV preparations led to a significant increase in the levels of intracellular syntenin and syndecan-1 compared with BCR-ABL1$^+$ BA/F3 cells exposed to sEVs prepared from WT MSCs ($P = .02$ [syntenin], $P = .04$, [syndecan-1]; Figure 4A). Prior treatment of BCR-ABL1$^+$ BA/F3 cells exposed to sEVs from *Plekhm1* KO vs WT MSCs with bortezomib and cycloheximide to inhibit protein degradation and synthesis, respectively, confirmed that the elevated levels of syntenin after exposure to *Plekhm1* KO sEVs were due to uptake of the sEV-derived cargo (supplemental Figure 7A). In addition, exposure of BCR-ABL1$^+$ BA/F3 cells to *Plekhm1* KO sEV preparations significantly increased the phosphorylation of AKT on the Ser473 residue compared with sEVs prepared from WT MSCs ($P = .03$; Figure 4B). AKT phosphorylation on Ser473 is required for maximal AKT activation controlling cell cycle, proliferation, and survival.[39,40] This effect was reversed after treatment of BA/F3 cells with dynasore to inhibit endocytosis[41] (Figure 4B; supplemental Figure 7B). In addition, combination treatment with a syntenin inhibitor, PDZ1i,[42] and the BCR-ABL1–targeting tyrosine kinase inhibitor dasatinib reduced the viability of BCR-ABL1$^+$ BA/F3 cells more efficiently than dasatinib alone ($P = .008$; supplemental Figure 7C). Furthermore, we found a trend toward higher expression of syntenin in BM cells of *Plekhm1* KO compared with WT mice with B-ALL but not CML (supplemental Figure 7D-E).

Syndecan-1 forms complexes with growth factor receptors and/or integrins on the cell surface, resulting in their stabilization and enhancement of their downstream signaling pathways.[43,44] In agreement with this, we observed a significant increase in phosphorylation of FAK on residue Tyr397 in BCR-ABL1$^+$ BA/F3 cells after exposure to *Plekhm1* KO compared with sEVs prepared from WT MSCs, whereby FAK is known to serve as a mediator of activated integrin signal transduction[45] ($P = .03$; Figure 4C). Expression of integrins αV, β3, α5, and α2b on the surface of B-ALL cells isolated from WT or *Plekhm1* KO mice, however, did not reveal any differences (supplemental Figure 8A-B). In line with the known role of FAK,[46,47] syndecan,[38] and syntenin[48] for cell mobility, the migration of BCR-ABL1$^+$ BA/F3 cells treated with sEVs derived from *Plekhm1* KO compared with WT MSCs was significantly increased ($P = .02$; Figure 4D). To test directly whether sEV preparations from *Plekhm1* KO MSCs promoted the acceleration of B-ALL, we treated BCR-ABL1–transduced WT BM cells with WT or *Plekhm1* KO sEVs and transplanted these pretreated BM cells into WT recipient mice. This did not lead to differences in the tumor load in the form of GFP$^+$ (BCR-ABL1$^+$) BP-1$^+$ cells in PB of the recipient mice (supplemental Figure 8C). However, a strong trend toward shortened survival of mice that had received BCR-ABL1$^+$ BM cells previously exposed to *Plekhm1* KO compared with WT sEVs was observed ($P = .06$; Figure 4E). Previous exposure of LICs to *Plekhm1* KO but not WT sEVs also led to a trend toward an increase of pAKT Ser473 in GFP$^+$ (BCR-ABL1)$^+$ BP-1$^+$ cells from recipient mice with B-ALL (Figure 4F; supplemental Figure 8D).

Testing possible differences between BCR-ABL1$^+$ and BCR-ABL1$^-$ B-ALL, we showed that transplantation of the human BCR-ABL1$^+$ B-ALL cell line SUPB15, previously exposed to sEVs from *Plekhm1* KO compared with WT MSCs, but not the equally treated BCR-ABL1$^-$ B-ALL cell line NALM6 into NOD SCID IL-2 receptor γ KO mice (supplemental Figure 7H-I), led to a strong trend toward shortened survival ($P = .057$; Figure 4G; supplemental Figure 8E-G). In summary, uptake of sEVs derived from *Plekhm1* KO compared with WT MSCs led to an increase in the levels of syntenin, syndecan-1, pFAK, and pAKT Ser473 in B-ALL cells, an increase in migration of B-ALL cells, and likely acceleration of B-ALL

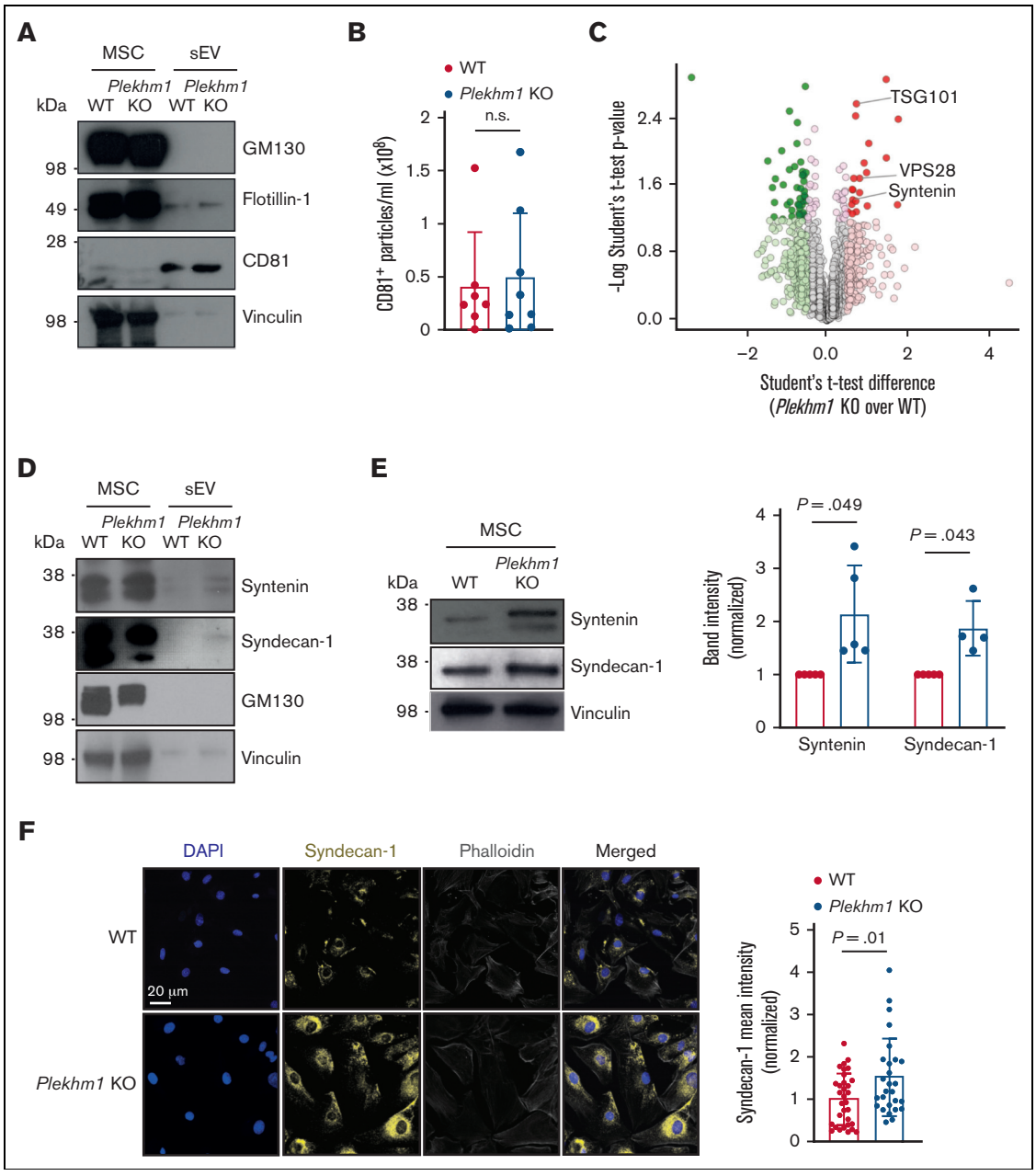

Figure 3. *Plekhm1* KO MSCs release syntenin- and syndecan-1–enriched sEVs. (A) Representative immunoblot showing expression of GM130, CD81, and flotillin-1 in WT or *Plekhm1* KO MSCs or sEVs derived from equal numbers of WT or *Plekhm1* KO MSCs. Vinculin was used as a loading control for MSCs and as a negative marker for sEVs. The data represent results from 4 independent experiments. (B) Quantification of $CD81^+$ particles/mL ($\times 10^8$) in sEVs derived from WT (red) or *Plekhm1* KO (blue) MSCs (WT n = 7; *Plekhm1* KO n = 8; *t* test). The values are normalized to the number of donor MSCs. (C) Volcano plot showing protein expression in sEVs from WT vs *Plekhm1* KO MSCs. Samples were normalized for protein concentration before mass spectrometry. The x-axis indicates the difference in protein abundance between *Plekhm1* KO and WT MSCs, whereas the y-axis indicates the −log *P* value (Student *t* test). Proteins in dark red are expressed significantly more highly and in dark green significantly less in sEV from *Plekhm1* KO vs WT MSCs. The data represent the results of 4 biological replicates (*t* test). (D) Representative immunoblot showing expression of syntenin, syndecan-1, and GM130 in WT vs *Plekhm1* KO MSCs or sEVs derived from WT or *Plekhm1* KO MSCs. The data (syndecan-1) represent results from 4 independent experiments. (E) Representative immunoblot (left) and its quantification (right) showing expression of syntenin and syndecan-1 in WT or *Plekhm1* KO MSCs. The values are normalized to the WT for each individual experiment and are the results of 5 (syntenin) or 4 (syndecan-1) biological replicates (multiple *t* tests). (F) Representative immunofluorescence images of syndecan-1 staining on WT or *Plekhm1* KO MSCs (left). The nuclei are counterstained with DAPI (blue) (left). The scale bar depicts 20 μm. The quantification of syndecan-1 fluorescence intensity in WT (red) or *Plekhm1* KO (blue) MSCs, normalized to the average value in WT MSCs is shown on the right. The data represent the results of 4 biological replicates (right) (*t* test). DAPI, 4′,6-diamidino-2-phenylindole.

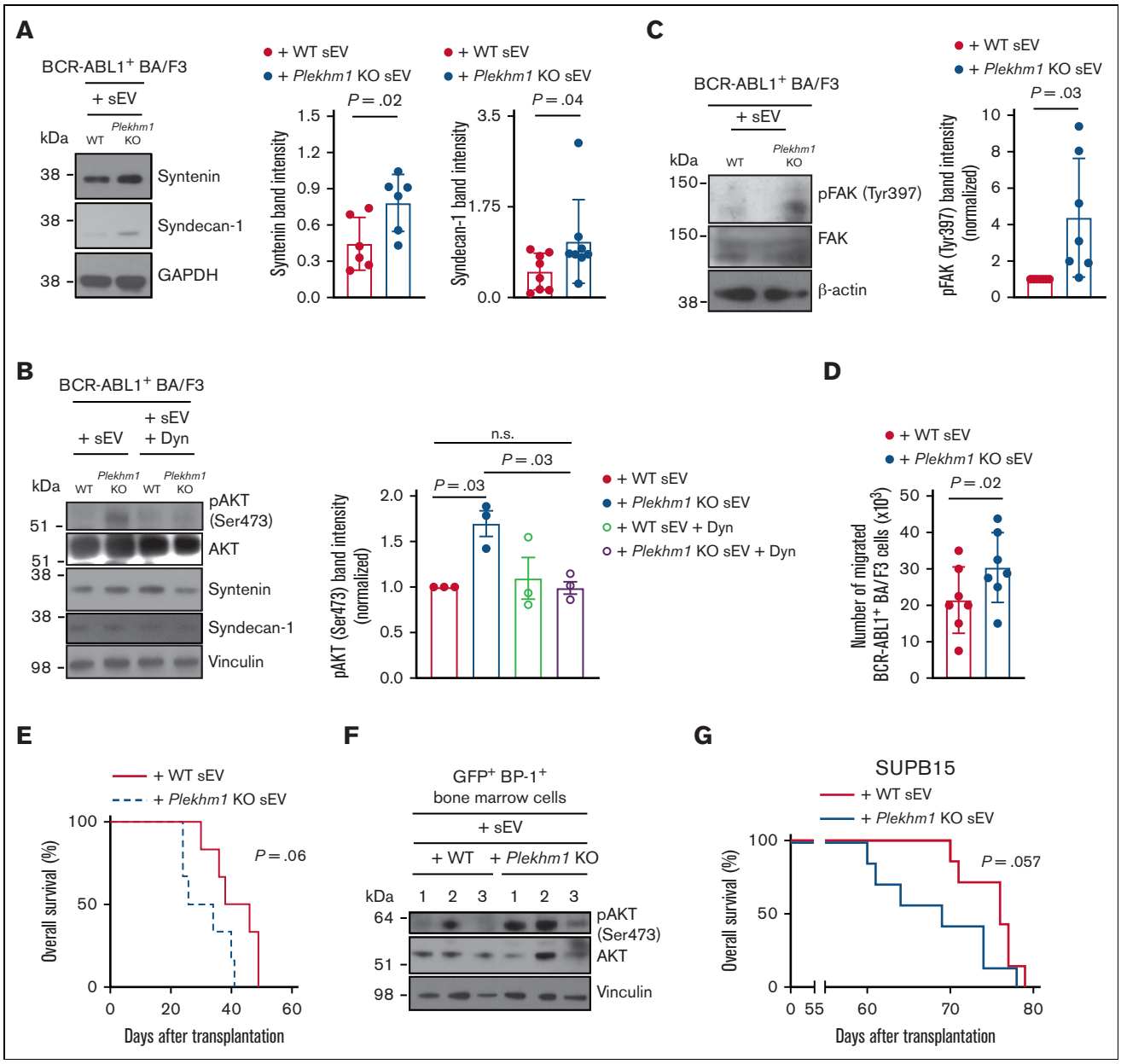

Figure 4. sEVs derived from *Plekhm1* KO MSCs alter signaling in B-ALL cells and may promote B-ALL progression. (A) Representative immunoblot showing the expression of syntenin and syndecan-1 in BCR-ABL1$^+$ BA/F3 cells after a 40-minute exposure to sEVs derived from WT or *Plekhm1* KO MSCs (left). The quantification of syntenin (middle) and syndecan-1 (right) protein expression, normalized over the housekeeping protein GAPDH is shown on the right. The data represent the results of 6 (syntenin) or 7 (syndecan-1) independent experiments (*t* test). (B) Representative immunoblot showing the expression of pAKT (Ser473), AKT, syntenin, and syndecan-1 in BCR-ABL1$^+$ BA/F3 cells after exposure to sEVs from WT or *Plekhm1* KO MSCs with or without 20-μM dynasore for 6 hours (left) and quantification of pAKT (Ser473) expression (normalized to the +WT sEV control) (right). The data represent the results of 3 independent experiments (one-way ANOVA, Tukey multiple comparisons test). (C) Representative immunoblot showing the expression of pFAK (Tyr397) and FAK in BCR-ABL1$^+$ BA/F3 cells after exposure to WT or *Plekhm1* KO sEVs. The quantification of pFAK (Tyr397) expression, normalized over the housekeeping protein beta-actin, is shown on the right. The data represent the results of 7 independent experiments (*t* test). (D) Number of BCR-ABL1$^+$ BA/F3 cells after a 40-minute exposure to WT or *Plekhm1* KO sEVs, which migrated to the lower chamber of a transwell (5 μm pore size) within 6 hours. The medium in the upper vs the lower chambers of the transwell was substituted with 2% or 20% fetal bovine serum, respectively. (E) Kaplan-Meier style survival curve of mice transplanted with BCR-ABL1–transduced BM, which had previously been incubated for 1 hour with WT (red solid line) or *Plekhm1* KO (blue dashed line) sEVs (sEVs from donor MSCs were incubated with BCR-ABL1-transduced BM cells in a 1:5 ratio) and transplanted into WT recipient mice (+WT sEVs n = 6; +*Plekhm1* KO sEV n = 6; log-rank test). (F) Immunoblot showing pAKT (Ser473) and AKT expression in sorted primary GFP$^+$ (BCR-ABL1$^+$) BP-1$^+$ cells from the BM of WT recipient mice transplanted with BCR-ABL1–transduced BM cells previously exposed to WT or *Plekhm1* KO sEV from panel E. Each lane represents an individual mouse. (G) Kaplan-Meier style survival curve of NOD SCID interleukin-2 (IL-2) receptor γ KO mice transplanted with 1.5 × 10^6 SUBP15 cells, which had previously been incubated with WT (red line) or *Plekhm1* KO (blue line) sEVs (sEVs from donor MSCs were incubated with SUBP15 cells in a 1:5 ratio) for 1 hour (*P* = .057; +WT sEVs n = 7; +*Plekhm1* KO sEVs n = 7; Gehan-Breslow-Wilcoxon test). GAPDH, glyceraldehyde 3-phosphate dehydrogenase.

progression. This effect seemed more pronounced in BCR-ABL1$^+$ lymphoid rather than in BCR-ABL1$^+$ myeloid or BCR-ABL1$^-$ lymphoid leukemias.

TNF-α secreted by B-ALL cells perpetuated the sEV-associated circuit via regulation of PLEKHM1 expression in MSCs

Because B-ALL cells modify MSCs via the generation of tumor necrosis factor (TNF) α[24] and TNFα/*TNF* levels were higher in murine B-ALL vs AML and CML (supplemental Figure 9A), as well as in BCR-ABL1$^+$ SUPB15 compared with BCR-ABL1$^-$ NALM6 human B-ALL cell lines (supplemental Figure 9B-C), we tested whether the secretion of TNF-α by B-ALL cells may reproduce the phenotype observed in *Plekhm1* KO MSCs. Indeed, the treatment of WT MSCs with TNF-α led to increased phosphorylation of the NF-κB subunit p65 (supplemental Figure 9D). In addition, treatment with TNF-α or coculture of WT MSCs with BCR-ABL1$^+$ BA/F3 cells, separated by a membrane, decreased expression of PLEKHM1 in WT MSCs with concomitant upregulation of syntenin and syndecan-1 (Figure 5A; supplemental Figure 9E-F). Adalimumab, an antibody inhibiting TNF-α, rescued PLEKHM1 reduction in MSCs after coculture with BCR-ABL1$^+$ BA/F3 cells (Figure 5B; supplemental Figure 9G).

The decrease of PLEKHM1 after TNF-α treatment was already detectable in MSCs (supplemental Figure 10A) and in the stromal cell line MS5 (supplemental Figure 10B) after 30 minutes. In addition, the migration of BCR-ABL1$^+$ BA/F3 cells, which had been exposed to sEVs from MSCs ($P = .004$; Figure 5C) or MS5 (supplemental Figure 10C) cells, pretreated with TNF-α, was increased. Testing the qualitative effect of TNF-α on sEV production, we found that sEVs from WT MSCs, which had been treated with TNF-α, led to an upregulation of pFAK in sEV-exposed BCR-ABL1$^+$ BA/F3 cells ($P = .04$; Figure 5D).

With relevance to the human setting, we identified that exposure of HS5 cells, a human BM stroma cell line, to SUPB15 cells ($P = .04$; Figure 5E) and treatment of HS5 cells ($P = .001$; Figure 5F) and primary human MSCs ($P = .03$; Figure 5G) with human TNF-α also led to a reduction of PLEKHM1. Treatment of HS5 cells with TNF-α resulted in the release of sEVs with increased levels of their cargo, syntenin ($P = .05$; Figure 5H). Furthermore, TNF-α decreased levels of PLEKHM1 in MC3T3 cells, an osteoblast precursor cell line, but not in H5V cells or human umbilical vein endothelial cells, murine and human endothelial cell lines, respectively (supplemental Figure 11A-C).

Finally, in an effort to test whether the effect was specific to TNF-α, we demonstrated that treatment of MSCs (supplemental Figure 12A) or MS5 cells (supplemental Figure 12B) with IL-1β, another proinflammatory cytokine, caused a significant decrease in PLEKHM1 levels after 24 hours. Similar to TNF-α, *Il1b* was more highly expressed in SUPB15 compared with NALM6 cells (supplemental Figure 12C). In summary, these data demonstrate that secretion of TNF-α and other inflammatory cytokines such as IL-1β reduces expression of PLEKHM1 in murine and human MSCs and, in the case of TNF-α, alters the quality of sEVs secreted from MSCs. The altered sEV cargo affected migration and likely pFAK signaling in target leukemia cells, thereby maintaining a circuit that may perpetuate leukemia progression. A reduction of PLEKHM1 in response to TNF-α was also identified in osteoblastic but not endothelial cell lines.

The percentage of PLEKHM1$^+$ MSCs may be reduced in bone sections of human patients with B-ALL compared to CML

Testing the relevance of our findings in the human setting, we found the percentage of PLEKHM1$^+$ CD271$^+$ MSCs to be decreased in trephine biopsies of patients with B-ALL compared to CML ($P = .03$; Figure 6A-B; supplemental Figure 13A). The percentage of CD271$^+$ cells was significantly higher in sections from healthy individuals compared with patients with certain hematological malignancies (supplemental Figure 13B), whereas the percentage of PLEKHM1$^+$ cells was lowest in patients with B-ALL (supplemental Figure 13C). Although the number of analyzed patients is low, the data suggest that PLEKHM1 expression may also be decreased in human MSCs in B-ALL compared to CML, similar to our findings in mice.

Discussion

In the context of cancer, most studies have focused on cancer cell–derived exosomes or sEVs, which have the capacity to transform the tumor microenvironment.[31,32,49] Few studies and, to our knowledge, none in B-ALL have investigated the role of sEVs derived from the microenvironment.[50-52] Here, we demonstrate that deletion of *Plekhm1*, a central protein in the endolysosomal system, modulates the cargo of MSC-derived, that is, cancer cell–extrinsic, sEVs by increasing their loading with syntenin and syndecan-1. Uptake of this cargo decreases apoptosis and increases leukemia cell cycling. This promotes B-ALL progression and leukemia-initiating capacity via increased phosphorylation of FAK and AKT, specifically in the secondary transplantation setting, in which exposure of LICs to a *Plekhm1* KO BMM is prolonged. In turn, TNF-α and IL-1β, secreted by B-ALL and other leukemias,[53] decrease PLEKHM1 in murine and human MSCs and osteoblastic but not endothelial cells. However, given our observed differences in the phenotype of CML, AML vs B-ALL in a *Plekhm1* KO BMM and the predominance of the effect in BCR-ABL1$^+$ vs BCR-ABL1$^-$ B-ALL, we hypothesize that syndecan-1 and/or syntenin may have leukemia lineage- and/or oncogene-specific effects, as has been suspected.[38,54] These effects may contribute to the worse prognosis in BCR-ABL1$^+$ B-ALL.

Consistent with other reports on the involvement of vesicular trafficking–associated proteins for the regulation of EV cargo,[55] we discovered a potential role for PLEKHM1 in the loading of intraluminal vesicles with proteins such as syntenin and syndecan-1. In contrast, the levels of both proteins did not differ in our proteomics study of B-ALL cells from a WT vs a *Plekhm1* KO BMM, suggesting that their intracellular presence may be short but trigger the phosphorylation of AKT and FAK.

Syntenin and syndecan-1 have been suggested to stabilize growth factor receptors and/or integrins on the cell surface.[43,56,57] Consistently, we observed increased expression of pFAK[58] and pAKT downstream of integrin receptors in leukemia cells exposed to sEVs from a *Plekhm1* KO compared with a WT BMM, although expression levels of integrins did not differ. An effect of stabilization of growth factor receptors due to syntenin- and syndecan-1–loaded sEVs on AKT phosphorylation cannot be excluded. Consistent with our data, syndecan-1 was recently identified as an important mediator of CML progression in blast

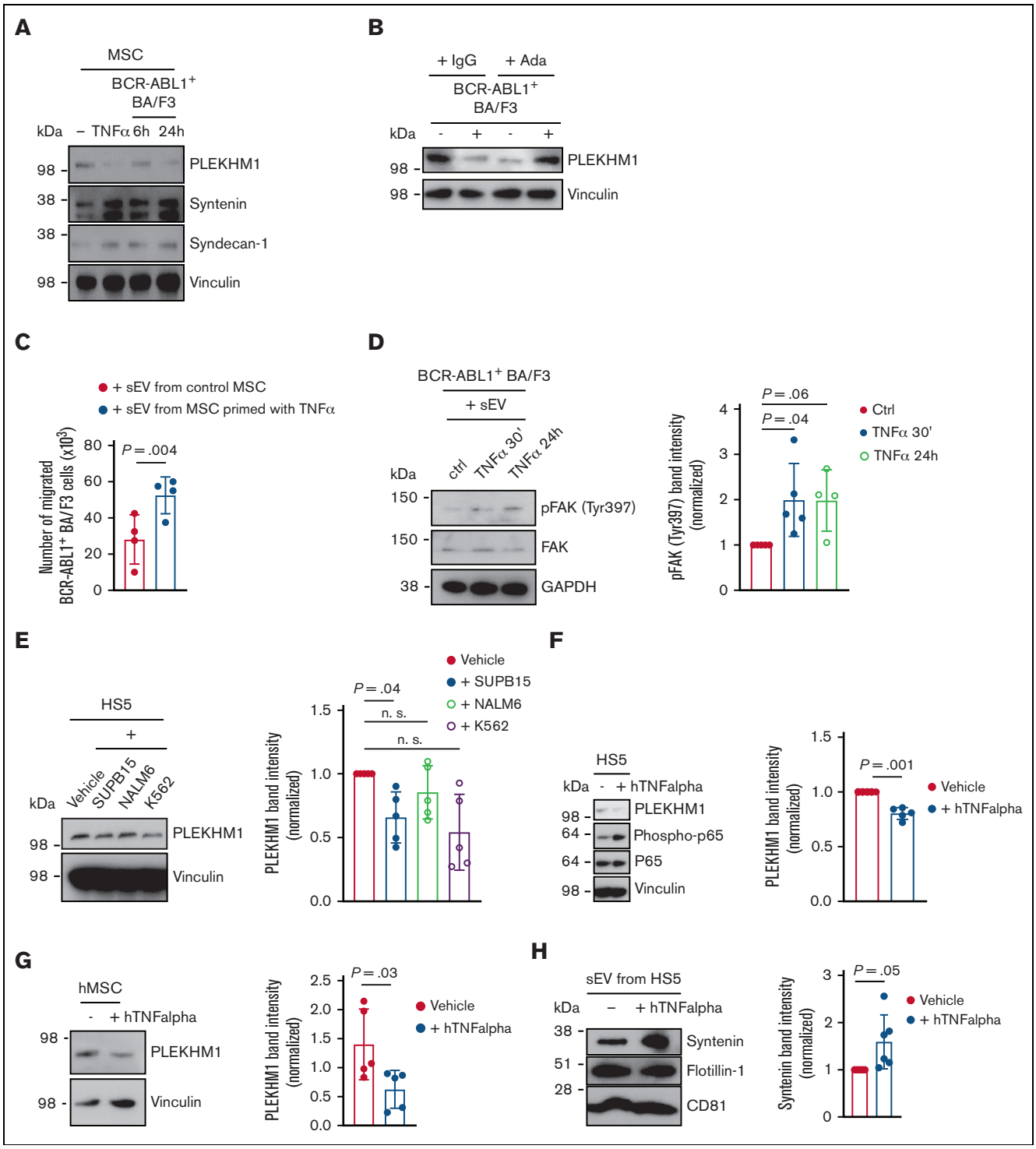

Figure 5. TNFα secreted by B-ALL cells perpetuates the sEV-associated circuit via regulation of PLEKHM1 expression in MSCs. (A) Representative immunoblot of PLEKHM1, syntenin, and syndecan-1 expression in WT MSCs treated with 15 ng/mL TNF-α for 24 hours or cocultured with BCR-ABL1$^+$ BA/F3 cells for 24 hours. The data represent the results of 4 independent experiments. (B) Representative immunoblot of PLEKHM1 expression in WT MSCs cocultured with or without BCR-ABL1$^+$ BA/F3 cells and treated with IgG control (IgG) or adalimumab (ada). The data represent the results of 6 independent experiments. (C) Number of BCR-ABL1$^+$ BA/F3 cells, which were exposed for 40 minutes to sEVs derived from untreated MSCs (control = ctrl) or MSCs treated with TNF-α for 24 hours and which migrated to the lower chamber of a transwell (5 μm pore size) within 6 hours. The medium in the upper vs the lower chambers of the transwell was substituted with 2% or 20% fetal bovine serum, respectively. The data represent the results of 4 independent experiments. (D) Representative immunoblot and its quantification showing expression of pFAK (Tyr397) and FAK in BCR-ABL1$^+$ BA/F3 cells after exposure to sEVs derived from untreated MSCs (control = ctrl), MSCs treated with TNF-α for 30 minutes or 24 hours. The values are normalized to the housekeeping protein GAPDH. The data represent the results of 4 to 5 independent experiments (one-way ANOVA, Dunnett multiple comparisons test). (E) Representative

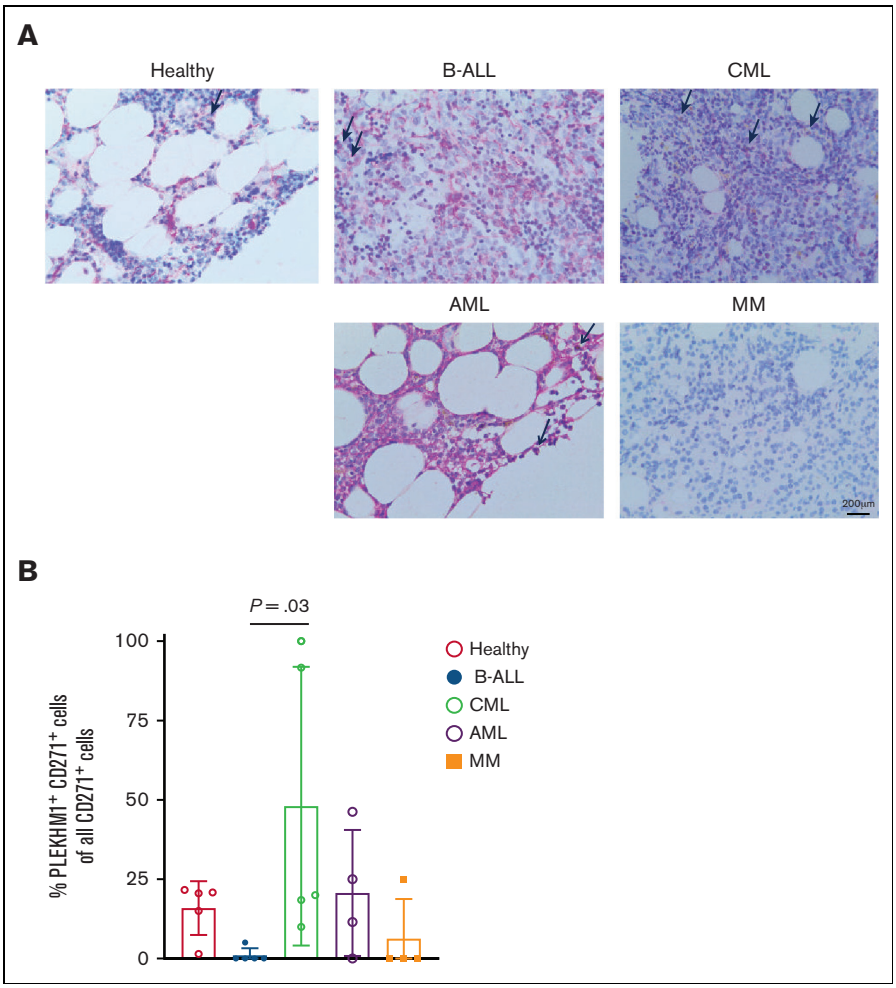

Figure 6. The percentage of PLEKHM1$^+$ MSCs may be reduced in bone sections of human patients with B-ALL compared to CML. (A) Representative bone sections of a healthy individual and human patients with B-ALL, CML, AML, or multiple myeloma (MM). The bone sections are stained with antibodies to CD271 (pink), labeling mesenchymal stroma cells, and PLEKHM1 (brown). The scale bar represents 200 µm. (B) Percentage of PLEKHM1$^+$ CD271$^+$ cells of all CD271$^+$ cells in bone sections of healthy individuals (n = 5) or patients with B-ALL (n = 5), CML (n = 5), AML (n = 4) or MM (n = 4) (one-way ANOVA, Tukey multiple comparisons test). The exact genotypes of the different leukemias are unknown.

crisis and to promote the migration and localization of CML progression in blast crisis cells while augmenting the activity of integrin β_7.[38]

Inflammatory cytokines, specifically TNF-α, have previously been implicated in the remodeling of the BMM[24] or the tumor microenvironment,[59,60] which, in turn, promoted tumor growth. Therefore, the net effect is similar to our study, although the mechanisms differ. TNF-α is known to promote sEV release and to modify their cargo,[61,62] but the described machinery did not involve proteins of the endosome generation and trafficking pathways.

Finally, autophagy inhibitors, such as hydroxychloroquine, have been used in combination with targeted therapies in clinical trials,[63] but caution must be exercised with regard to the development of novel autophagy inhibitors[64,65] because these treatments may also affect the release and quality of tumor-modifying exosomal cargo by cells of the microenvironment, endangering treatment success or negatively influencing cancer progression.

Taken together, our data suggest that quality control processes in cells of the tumor microenvironment are usurped by cancer cells to promote cancer progression. Although human patient numbers are small, our data suggest that PLEKHM1$^+$ MSCs may indeed be reduced in B-ALL but not in CML, likely because of higher TNF-α levels in B-ALL, explaining observed survival differences in *Plekhm1* KO mice with B-ALL vs CML. How the discovered pathways can be exploited therapeutically will be studied in depth in the future.

Acknowledgments

The authors thank the Quantitative Proteomics Unit (IBC2, Goethe University Frankfurt) for support on liquid chromatography–mass

Figure 5 (continued) immunoblot and its quantification showing expression of PLEKHM1 in HS5 cells after coculture with vehicle, SUPB15 (BCR-ABL1$^+$), NALM6 (BCR-ABL1$^-$), or K562 cells for 24 hours. The values are normalized to the housekeeping protein vinculin. The data represent the results of 5 independent experiments (one-way ANOVA, Dunnett multiple comparisons test). (F) Representative immunoblot and its quantification showing expression of PLEKHM1, phospho-p65, and p65 in HS5 cells treated with vehicle or 15 ng/mL human TNF-α (hTNF-α) for 24 hours. The results represent 5 independent experiments (*t* test). (G) Representative immunoblot and its quantification showing expression of PLEKHM1 in primary human MSCs treated with vehicle or 15 ng/mL hTNF-α for 24 hours. The results represent 5 independent experiments (*t* test). (H) Representative immunoblot and showing expression of syntenin, flotillin-1, and CD81 and quantification of syntenin in sEVs isolated from HS5 cells treated with vehicle or human TNF-α for 24 hours. The results represent 6 independent experiments (*t* test). GAPDH, glyceraldehyde 3-phosphate dehydrogenase.

spectrometry (LC-MS) instrumentation and the Deutsche Forschungsgemeinschaft (DFG) for funding the Orbitrap Lumos LC-MS system used in this study (FuG 403765277).

This work was supported by grant KR2072/6-1 from the DFG (to D.S.K.) and by the LOEWE Center for Cell and Gene Therapy Frankfurt (CGT) and institutional funds of the Georg-Speyer-Haus (to D.S.K.). The Georg-Speyer-Haus is funded jointly by the German Federal Ministry of Health and the Ministry of Higher Education, Research and the Arts of the State of Hessen (HMWK). CGT is funded by HMWK, reference number: III L 4 to 518/17.004 (2010).

Authorship

Contribution: C.K. and D.S.K. designed the experiments; C.K. and V.R.M. performed the in vitro and in vivo experiments; R.K., C.Z., J.B., R.S.P., and A.C.-P. assisted with experiments and critically discussed data; G.T. and C.M. performed the proteomics experiments; T.T. and B.G. performed the experiment involving AMNIS technology; K.B. performed the staining of human bone sections; D.G.M. and I.D. critically discussed data; L.-M. P. and H.B. provided human MSC; P.D.-P. helped with osteoclast differentiation; C.K. analyzed the data and wrote a first draft of the manuscript; D.S.K. supervised the research, analyzed data, and wrote the manuscript; and all authors critically read and approved the manuscript.

Conflict-of-interest disclosure: The authors declare no competing financial interests.

ORCID profiles: C.K., 0000-0002-2161-914X; V.R.M., 0000-0002-9296-9403; C.Z., 0000-0001-9384-1543; G.T., 0000-0002-5907-3947; T.T., 0000-0001-8659-8610; A.C.-P., 0000-0002-8946-2804; H.B., 0000-0003-0088-2675; D.G.M., 0000-0003-0353-6532; B.G., 0000-0003-2446-948X; D.S.K., 0000-0003-3603-1119.

Correspondence: Daniela S. Krause, Goethe University, c/o Georg-Speyer-Haus, Institute for Tumor Biology and Experimental Therapy, Paul-Ehrlich-Str. 42-44, 60596 Frankfurt am Main, Germany; email: krause@gsh.uni-frankfurt.de.

References

1. Inaba H, Greaves M, Mullighan CG. Acute lymphoblastic leukaemia. *Lancet*. 2013;381(9881):1943-1955.
2. Bernt KM, Hunger SP. Current concepts in pediatric Philadelphia chromosome-positive acute lymphoblastic leukemia. *Front Oncol*. 2014;4(54).
3. Leoni V, Biondi A. Tyrosine kinase inhibitors in BCR-ABL positive acute lymphoblastic leukemia. *Haematologica*. 2015;100(3):295-299.
4. Abou Dalle I, Kantarjian HM, Short NJ, et al. Philadelphia chromosome-positive acute lymphoblastic leukemia at first relapse in the era of tyrosine kinase inhibitors. *Am J Hematol*. 2019 Dec;94(12):1388-1395.
5. Mendez-Ferrer S, Bonnet D, Steensma DP, et al. Bone marrow niches in haematological malignancies. *Nat Rev Cancer*. 2020;20(5):285-298.
6. Karantanou C, Godavarthy PS, Krause DS. Targeting the bone marrow microenvironment in acute leukemia. *Leuk Lymphoma*. 2018;59(11):2535-2545.
7. Kollet O, Dar A, Shivtiel S, et al. Osteoclasts degrade endosteal components and promote mobilization of hematopoietic progenitor cells. *Nat Med*. 2006;12(6):657-664.
8. Cheung LC, Tickner J, Hughes AM, et al. New therapeutic opportunities from dissecting the pre-B leukemia bone marrow microenvironment. *Leukemia*. 2018;32(11):2326-2338.
9. Rajakumar SA, Papp E, Lee KK, et al. B cell acute lymphoblastic leukemia cells mediate RANK-RANKL-dependent bone destruction. *Sci Transl Med*. 2020;12(561).
10. Van Wesenbeeck L, Odgren PR, Coxon FP, et al. Involvement of PLEKHM1 in osteoclastic vesicular transport and osteopetrosis in incisors absent rats and humans. *J Clin Invest*. 2007;117(4):919-930.
11. McEwan DG, Popovic D, Gubas A, et al. PLEKHM1 regulates autophagosome-lysosome fusion through HOPS complex and LC3/GABARAP proteins. *Mol Cell*. 2015;57(1):39-54.
12. Mizushima N, Komatsu M. Autophagy: renovation of cells and tissues. *Cell*. 2011;147(4):728-741.
13. McEwan DG, Richter B, Claudi B, et al. PLEKHM1 regulates Salmonella-containing vacuole biogenesis and infection. *Cell Host Microbe*. 2015;17(1):58-71.
14. Marwaha R, Arya SB, Jagga D, Kaur H, Tuli A, Sharma M. The Rab7 effector PLEKHM1 binds Arl8b to promote cargo traffic to lysosomes. *J Cell Biol*. 2017;216(4):1051-1070.
15. Tabata K, Matsunaga K, Sakane A, Sasaki T, Noda T, Yoshimori T. Rubicon and PLEKHM1 negatively regulate the endocytic/autophagic pathway via a novel Rab7-binding domain. *Mol Biol Cell*. 2010;21(23):4162-4172.
16. Hessvik NP, Llorente A. Current knowledge on exosome biogenesis and release. *Cell Mol Life Sci*. 2018;75(2):193-208.
17. Krause DS, Fulzele K, Catic A, et al. Differential regulation of myeloid leukemias by the bone marrow microenvironment. *Nat Med*. 2013;19(11):1513-1517.
18. Minciacchi VR, You S, Spinelli C, et al. Large oncosomes contain distinct protein cargo and represent a separate functional class of tumor-derived extracellular vesicles. *Oncotarget*. 2015;6(13):11327-11341.
19. Zanetti C, Kumar R, Ender J, et al. The age of the bone marrow microenvironment influences B-cell acute lymphoblastic leukemia progression via CXCR5-CXCL13. *Blood*. 2021;138(19):1870-1884.

20. Cobaleda C, Schebesta A, Delogu A, Busslinger M. Pax5: the guardian of B cell identity and function. *Nat Immunol*. 2007;8(5):463-470.
21. Kozmik Z, Wang S, Dorfler P, Adams B, Busslinger M. The promoter of the CD19 gene is a target for the B-cell-specific transcription factor BSAP. *Mol Cell Biol*. 1992;12(6):2662-2672.
22. Alt FW, Zhang Y, Meng FL, Guo C, Schwer B. Mechanisms of programmed DNA lesions and genomic instability in the immune system. *Cell*. 2013;152(3):417-429.
23. Azab E, Chandler KB, Uda Y, et al. Osteocytes control myeloid cell proliferation and differentiation through Gsalpha-dependent and -independent mechanisms. *Faseb J*. 2020;34(8):10191-10211.
24. Verma D, Zanetti C, Godavarthy PS, et al. Bone marrow niche-derived extracellular matrix-degrading enzymes influence the progression of B-cell acute lymphoblastic leukemia. *Leukemia*. 2020;34(6):1540-1552.
25. Tikhonova AN, Dolgalev I, Hu H, et al. The bone marrow microenvironment at single-cell resolution. *Nature*. 2019;569(7755):222-228.
26. Polak R, de Rooij B, Pieters R, den Boer ML. B-cell precursor acute lymphoblastic leukemia cells use tunneling nanotubes to orchestrate their microenvironment. *Blood*. 2015;126(21):2404-2414.
27. Houlihan DD, Mabuchi Y, Morikawa S, et al. Isolation of mouse mesenchymal stem cells on the basis of expression of Sca-1 and PDGFR-alpha. *Nat Protoc*. 2012;7(12):2103-2111.
28. Fader CM, Colombo MI. Autophagy and multivesicular bodies: two closely related partners. *Cell Death Differ*. 2009;16(1):70-78.
29. Kobayashi T, Vischer UM, Rosnoblet C, et al. The tetraspanin CD63/lamp3 cycles between endocytic and secretory compartments in human endothelial cells. *Mol Biol Cell*. 2000;11(5):1829-1843.
30. Xu J, Camfield R, Gorski SM. The interplay between exosomes and autophagy - partners in crime. *J Cell Sci*. 2018;131(15).
31. Kumar B, Garcia M, Weng L, et al. Acute myeloid leukemia transforms the bone marrow niche into a leukemia-permissive microenvironment through exosome secretion. *Leukemia*. 2018;32(3):575-587.
32. Johnson SM, Dempsey C, Chadwick A, et al. Metabolic reprogramming of bone marrow stromal cells by leukemic extracellular vesicles in acute lymphoblastic leukemia. *Blood*. 2016;128(3):453-456.
33. Vagner T, Spinelli C, Minciacchi VR, et al. Large extracellular vesicles carry most of the tumour DNA circulating in prostate cancer patient plasma. *J Extracell Vesicles*. 2018;7(1):1505403.
34. Shabbir A, Cox A, Rodriguez-Menocal L, Salgado M, Van Badiavas E. Mesenchymal stem cell exosomes induce proliferation and migration of normal and chronic wound fibroblasts, and enhance angiogenesis in vitro. *Stem Cell Dev*. 2015;24(14):1635-1647.
35. Tertel T, Gorgens A, Giebel B. Analysis of individual extracellular vesicles by imaging flow cytometry. *Methods Enzymol*. 2020;645:55-78.
36. Kostelansky MS, Sun J, Lee S, et al. Structural and functional organization of the ESCRT-I trafficking complex. *Cell*. 2006;125(1):113-126.
37. Baietti MF, Zhang Z, Mortier E, et al. Syndecan-syntenin-ALIX regulates the biogenesis of exosomes. *Nat Cell Biol*. 2012;14(7):677-685.
38. Spinler K, Bajaj J, Ito T, et al. A stem cell reporter based platform to identify and target drug resistant stem cells in myeloid leukemia. *Nat Commun*. 2020;11(1):5998.
39. Verma D, Kumar R, Pereira RS, et al. Vitamin K antagonism impairs the bone marrow microenvironment and hematopoiesis. *Blood*. 2019;134(3):227-238.
40. Liu P, Begley M, Michowski W, et al. Cell-cycle-regulated activation of Akt kinase by phosphorylation at its carboxyl terminus. *Nature*. 2014;508(7497):541-545.
41. Preta G, Cronin JG, Sheldon IM. Dynasore - not just a dynamin inhibitor. *Cell Commun Signal*. 2015;13:24.
42. Pradhan AK, Maji S, Bhoopathi P, et al. Pharmacological inhibition of MDA-9/syntenin blocks breast cancer metastasis through suppression of IL-1β. *Proc Natl Acad Sci U S A*. 2021;118(21):e2103180118.
43. Beauvais DM, Rapraeger AC. Syndecan-1 couples the insulin-like growth factor-1 receptor to inside-out integrin activation. *J Cell Sci*. 2010;123(Pt 21):3796-3807.
44. Wang H, Jin H, Rapraeger AC. Syndecan-1 and syndecan-4 capture epidermal growth factor receptor family members and the alpha3beta1 integrin via binding sites in their ectodomains: novel synstatins prevent kinase capture and inhibit alpha6beta4-integrin-dependent epithelial cell motility. *J Biol Chem*. 2015;290(43):26103-26113.
45. Parsons JT. Focal adhesion kinase: the first ten years. *J Cell Sci*. 2003;116(Pt 8):1409-1416.
46. Tse KW, Dang-Lawson M, Lee RL, et al. B cell receptor-induced phosphorylation of Pyk2 and focal adhesion kinase involves integrins and the Rap GTPases and is required for B cell spreading. *J Biol Chem*. 2009;284(34):22865-22877.
47. Glodek AM, Le Y, Dykxhoorn DM, et al. Focal adhesion kinase is required for CXCL12-induced chemotactic and pro-adhesive responses in hematopoietic precursor cells. *Leukemia*. 2007;21(8):1723-1732.
48. Kashyap R, Roucourt B, Lembo F, et al. Syntenin controls migration, growth, proliferation, and cell cycle progression in cancer cells. *Front Pharmacol*. 2015;6:241.
49. Peinado H, Alečković M, Lavotshkin S, et al. Melanoma exosomes educate bone marrow progenitor cells toward a pro-metastatic phenotype through MET. *Nat Med*. 2012;18(6):883-891.

50. Roccaro AM, Sacco A, Maiso P, et al. BM mesenchymal stromal cell-derived exosomes facilitate multiple myeloma progression. *J Clin Invest*. 2013;123(4):1542-1555.

51. Crompot E, Van Damme M, Pieters K, et al. Extracellular vesicles of bone marrow stromal cells rescue chronic lymphocytic leukemia B cells from apoptosis, enhance their migration and induce gene expression modifications. *Haematologica*. 2017;102(9):1594-1604.

52. Javidi-Sharifi N, Martinez J, English I, et al. FGF2-FGFR1 signaling regulates release of Leukemia-Protective exosomes from bone marrow stromal cells. *Elife*. 2019:8.

53. Sugiyama H, Inoue K, Ogawa H, et al. The expression of IL-6 and its related genes in acute leukemia. *Leuk Lymphoma*. 1996;21(1-2):49-52.

54. Leblanc R, Fares J, Goubard A, et al. A syntenin-deficient microenvironment educates AML for aggressiveness. *bioRxiv*. 2021.

55. Gudbergsson JM, Johnsen KB. Exosomes and autophagy: rekindling the vesicular waste hypothesis. *J Cell Commun Signal*. 2019;13(4):443-450.

56. Beauvais DM, Ell BJ, McWhorter AR, Rapraeger AC. Syndecan-1 regulates alphavbeta3 and alphavbeta5 integrin activation during angiogenesis and is blocked by synstatin, a novel peptide inhibitor. *J Exp Med*. 2009 Mar 16;206(3):691-705.

57. Dasgupta S, Menezes ME, Das SK, et al. Novel role of MDA-9/syntenin in regulating urothelial cell proliferation by modulating EGFR signaling. *Clin Cancer Res*. 2013;19(17):4621-4633.

58. Kumar R, Pereira RS, Zanetti C, et al. Specific, targetable interactions with the microenvironment influence imatinib-resistant chronic myeloid leukemia. *Leukemia*. 2020;34(8):2087-2101.

59. Kulbe H, Thompson R, Wilson JL, et al. The inflammatory cytokine tumor necrosis factor-alpha generates an autocrine tumor-promoting network in epithelial ovarian cancer cells. *Cancer Res*. 2007;67(2):585-592.

60. Popivanova BK, Kitamura K, Wu Y, et al. Blocking TNF-alpha in mice reduces colorectal carcinogenesis associated with chronic colitis. *J Clin Invest*. 2008;118(2):560-570.

61. Wang K, Ye L, Lu H, et al. TNF-alpha promotes extracellular vesicle release in mouse astrocytes through glutaminase. *J Neuroinflammation*. 2017;14(1):87.

62. Chaudhuri AD, Dastgheyb RM, Yoo SW, et al. TNFalpha and IL-1beta modify the miRNA cargo of astrocyte shed extracellular vesicles to regulate neurotrophic signaling in neurons. *Cell Death Dis*. 2018;9(3):363.

63. Horne GA, Stobo J, Kelly C, et al. A randomised phase II trial of hydroxychloroquine and imatinib versus imatinib alone for patients with chronic myeloid leukaemia in major cytogenetic response with residual disease. *Leukemia*. 2020;34(7):1775-1786.

64. Baquero P, Dawson A, Mukhopadhyay A, et al. Targeting quiescent leukemic stem cells using second generation autophagy inhibitors. *Leukemia*. 2019;33(4):981-994.

65. Ding L, Zhang W, Yang L, et al. Targeting the autophagy in bone marrow stromal cells overcomes resistance to vorinostat in chronic lymphocytic leukemia. *Onco Targets Ther*. 2018;11:5151-5170.